Applied Catalysis B: Environmental 148–149 (2014) 106–113

Contents lists available at ScienceDirect

Applied Catalysis B: Environmental

journal homepage: www.elsevier.com/locate/apcatb

Pd/transition metal oxides functionalized ZSM-5 single crystals with *b*-axis aligned mesopores: Efficient and long-lived catalysts for benzene combustion☆

Fujian Liu[a,b], Shufeng Zuo[a], Chao Wang[a], Jiantao Li[c], Feng-Shou Xiao[b], Chenze Qi[a,*]

[a] *Key Laboratory of Alternative Technologies for Fine Chemicals Process of Zhejiang Province, Department of Chemistry, Shaoxing University, Shaoxing 312000, PR China*
[b] *Department of Chemistry, Zhejiang University, Hangzhou 310007, PR China*
[c] *Fushun Research Institute of Petroleum and Petrochemicals, SINOPEC, Fushun 113001, PR China*

ARTICLE INFO

Article history:
Received 18 June 2013
Received in revised form 20 October 2013
Accepted 28 October 2013
Available online 5 November 2013

Keywords:
Mesoporous zeolites
VOCs removing
b-axis aligned mesopores
Amphiphilic copolymer
Self-assembly

ABSTRACT

A series of PdO/transition metal oxides functionalized mesoporous ZSM-5 single crystals with *b*-axis aligned mesopores (*x*%Pd/*x*%M-ZSM-5-OMs) have been successfully prepared from self-assembly of the designed cationic amphiphilic copolymer of polystyrene-*co*-poly4-vinylpyridine (C-PSt-*co*-P4VP) with ZSM-5 zeolite precursor based on their strong positive-negative charge interaction under high temperature hydrothermal conditions. Characterizations of XRD patterns showed that *x*%Pd/*x*%M-ZSM-5-OMs exhibit good crystallinity with typical MFI zeolite characters; N_2 isotherms showed that *x*%Pd/*x*%M-ZSM-5-OMs have large BET surface areas and mesopore volumes. SEM images showed the single crystal structure of *x*%Pd/*x*%M-ZSM-5-OMs, which have abundant and *b*-axis aligned mesopores, running through the whole zeolite crystals. TEM images further confirmed *b*-axis aligned mesopores, and good dispersion of active sites with high degree of crystallinity in *x*%Pd/*x*%M-ZSM-5-OMs. XPS spectra showed that transition metal oxides and PdO active species have been successfully loaded into ZSM-5-OM support. H_2–TPR curves showed the low reduction temperatures of PdO and transition metal species in *x*%Pd/*x*%M-ZSM-5-OMs, which was favorable for the enhancement of their abilities for VOCs combustion. Catalytic tests showed that *x*%Pd/*x*%M-ZSM-5-OMs exhibit good catalytic activities and long catalytic lives for benzene combustion under rather mild conditions in comparison with that of *x*%Pd/*x*%M-ZSM-5, which would be very important for the wide applications of zeolites with controlled mesopores in the areas of VOCs oxidation.

1. Introduction

Crystalline aluminosilicates zeolites such as ZSM-5, Y and Beta have been widely used as efficient and stable heterogeneous catalysts and catalyst supports in the areas of petrochemistry and fine chemicals synthesis because of their unique characters such as large BET surface areas, uniform and intricate micropores, strong acid strength, and excellent shape-selective catalysis property [1–6]. However, their relatively small solo micropores severely constrain the mass transfer of heavy reactants to the active sites located within their micropores, which largely constrains their catalytic activities and lives for bulky molecular transformation [1,2,7–10]. The usage of zeolite nanocrystals partially overcomes the diffusion problem of conventional zeolites. However, the separation of zeolite nanocrystals from a reaction mixture is usually complicated [11,12].

The introduction of mesopores into zeolites develops a completely new way to overcome the problems of mass transfer, coking and sintering, and bulky molecular transformation for traditional zeolite catalysts, and tremendous efforts have been made to develop zeolites with opened and controlled mesopores in these years [13–20]. Mesoporous zeolites were initially synthesized by using nanosized or ordered nanoporous carbon as the hard templates, which usually lead to formation of unconnected mesopores in zeolites or the mesopores aggregated by zeolites nanocrystals. However, the high cost and complicated synthetic procedures of the hard template route largely constrain their wide industrial applications [16,21,22]. The usage of water soluble polymers such as polyquaternary ammonium surfactants as soft templates lead to the development of a cost-effective method for synthesis of

* Corresponding author.
E-mail address: qichenze@usx.edu.cn (C. Qi).

0926-3373/$ – see front matter.
http://dx.doi.org/10.1016/j.apcatb.2013.10.054

zeolites with opened and disordered mesopores, which will be potentially important for their wide applications in industry [18]. Up to now, one of the key challenges in mesoporous zeolites synthesis is obtaining the zeolites with controlled and opened mesopores, which may improve the diffusion and selective adsorption of bulky substrates during catalytic reactions, resulting in further enhancement of catalytic performances and lives.

Recently, Ryoo et al. successfully synthesized novel and ordered single-unit-cell zeolite nanosheets by using designed bifunctional surfactants for the first time [8,23,24], which offers great opportunity for preparation of long-lived hierarchical zeolite catalysts with controlled mesostructures, superior mass transfer property and catalytic activities for bulky substrates [25–27]. However, the resulted zeolite nanosheets usually lead to their complicated separation from reaction media and relatively low hydrothermal stabilities [28]. Very recently, our group successfully synthesized hydrothermally stable ZSM-5 single crystals with controlled and opened mesopores (ZSM-5-OM) by using designed amphiphilic copolymers (C-PSt-*co*-P4VP) as a template, which showed novel *b*-axis-aligned mesopore (ZSM-5-OM) channels, running through the whole ZSM-5 single crystals. These unique characters result in its excellent catalytic activities and recyclability for conversion of bulky organic molecules [28]. We report here that ZSM-5-OM acted as an efficient and stable support for loading with Pd and various transition metal oxides (*x*%Pd/*x*%M-ZSM-5-OMs) with excellent catalytic activities and long lives for benzene combustion under rather mild conditions (220 °C) in comparison with that of Pd and transition metal oxides supported on conventional ZSM-5. The enhanced catalytic performances found in *x*%Pd/*x*%M-ZSM-5-OMs is attributed to their unique characters including abundant *b*-axis-aligned mesopores, nanosized and well dispersed active sites, and the high concentration of active oxygen species. It is well known that benzene and other type of volatile organic compounds (VOCs) were the major components in air pollutants from motor vehicles and industrial processes as well as indoor decoration, which greatly threat human health and have received considerable attention in these years [29–37]. The successful preparation of *x*%Pd/*x*%M-ZSM-5-OMs will be potentially important for the wide applications of mesoporous zeolites with controlled mesostructrue in the area of removing VOCs in our modern lives.

2. Experimental details

2.1. Chemicals and regents

All of the reagents were of analytical grade and used as purchased without further purification. Copolymer of polystyrene-*co*-4-polyvinylpyridine (PSt-*co*-P4VP), methyl iodide, and tetrapropyl ammonium hydroxide (TPAOH, 19.5 wt%), were purchased from Sigma-Aldrich Company, Ltd. (USA). DMF, petroleum ether, tetraethyl orthosilicate (TEOS), benzene, $NaAlO_2$, NaOH, $Ce(NO_3)_3{\cdot}6H_2O$, $PdCl_2$, $Y(NO_3)_3{\cdot}6H_2O$, $La(NO_3)_3{\cdot}6H_2O$, $Pr(NO_3)_3{\cdot}3H_2O$, $Nd(NO_3)_3{\cdot}3H_2O$ were purchased from Tianjin Guangfu Chemical Reagent.

2.2. Synthesis of ZSM-5-OM

ZSM-5-OM was synthesized from self assembly of ZSM-5 zeolite precursor with cationic copolymer of C-polystyrene-*co*-4-polyvinylpyridine (C-PSt-*co*-P4VP), hydrothermal treatment at 180 °C and calcination at 550 °C. C-PSt-*co*-P4VP was synthesized from the treatment of PSt-*co*-P4VP with CH_3I at room temperature in DMF solvent under darkness. As a typical run, 2.0 g of PSt-*co*-P4VP was dispersed into 40 mL of DMF, followed by addition of 1.2 mL of methyl-iodide under conditions of darkness, after stirring of the mixture for 20 h at room temperature, the cationic copolymer template of C-PSt-*co*-P4VP could be collected from extraction with petroleum ether, filtration, washing with large amount of petroleum ether, and drying at 120 °C for 5 h.

ZSM-5-OM was synthesized by using TPAOH and C-PSt-*co*-P4VP as dual templates. Typically, 0.16 g of $NaAlO_2$ and 0.02 g of NaOH were dissolved into 26 mL of TPAOH, followed by addition of 14.0 mL of TEOS and 40 mL of water, after stirring the mixture at room temperature for 6 h and hydrothermal treatment at 100 °C for 2 h, a clear zeolite solution was obtained. Meanwhile, 4.0 g of C-PSt-*co*-P4VP was dissolved into a mixture containing 15 mL of water and 5 mL of TPAOH, giving a C-PSt-*co*-P4VP solution with dark blue color. The resulted ZSM-5 zeolite solution was slowly added into the C-PSt-*co*-P4VP aqueous solution, after vigorous stirring for 48 h at room temperature, the mixture was transferred into an autoclave for crystallization at 180 °C for 3–4 days. ZSM-5-OM could be collected by filtration, washing with large amount of water and calcination at 550 °C for 5 h.

For comparison, conventional ZSM-5 was synthesized under the same condition, but without addition of C-PSt-*co*-P4VP template.

2.3. Synthesis of transition metal oxides loaded ZSM-5-OM

Transition metal oxides functionalized ZSM-5-OM were synthesized by dipping ZSM-5-OM into an aqueous solution containing various transition metal ions, drying at 180 °C, and calcination at 400 °C for 2 h. As a typical run for synthesis of 6%La-ZSM-5-OM, 1.0 g of ZSM-5-OM with the particle sizes ranging for 40 to 60 mesh was dispersed into 1.0–2.0 mL of aqueous solution containing of 0.35 mmol of $La(NO_3)_2{\cdot}4H_2O$ for 12 h. After drying of the sample at 180 °C, and calcination at 400 °C for 2 h, LaO_x functionalized ZSM-5-OM of 6%La-ZSM-5-OM was obtained.

2.3.1. Preparation of 0.2%Pd/6%La-ZSM-5-OM

For further synthesis of 0.2%Pd/6%La-ZSM-5-OM, 0.5 g of 6%La-ZSM-5-OM was dipped into a solution containing of 2.5 mL of water and 1 mg of $PdCl_2$ for 12 h, the sample could be obtained from the treatment by irradiation with infrared lamp, reduction with hydrazine hydrate, and calcination at 400 °C for 2 h.

2.4. Characterizations

X-ray powder diffraction (XRD) of samples was recorded on a Rigaku D/max2550 PC powder diffractometer using nickel-filtered Cu $K\alpha$ radiation in the range of $4^\circ \leq 2\theta \leq 40^\circ$. The X-ray tube was operated at 40 kV and 300 mA. The specific surface areas (S_{BET}), total pore volumes, micropore volumes (V_{mic}) and micropore area (A_{mic}) of the samples was obtained from N_2 adsorption isotherms at −195.8 °C using a TristarII3020 apparatus of Micromeritics Company. Before measurements, the samples were outgassed at 200 °C under vacuum for 6 h. The pore-size distribution for mesopores was calculated using the Barrett–Joyner–Halenda (BJH) model. The inductively coupled plasma (ICP) was performed on a Perkin-Elmer 3300 DV for determination of the contents of various transition metal oxides and PdO_x in ZSM-5-OM. Transmission electron microscopy (TEM) experiments were performed on a JEM-3010 electron microscope (JEOL, Japan) with an acceleration voltage of 300 kV. SEM images were performed on JEOL 6335F field emission scanning electron microscope (FESEM) attached with a Thermo Noran EDX detector and Tecnai T12 transmission electron microscopy. XPS spectra were performed on a Thermo ESCALAB 250 with Al $K\alpha$ radiation, and binding energies were calibrated using the C_{1s} peak at 284.9 eV. Temperature programmed reduction (TPR) measurements were carried out on CHEMBET-3000 (Quantachrome, USA) instrument to observe reducibility of the catalysts. Before the measurement, 50 mg catalyst was pretreated at 300 °C

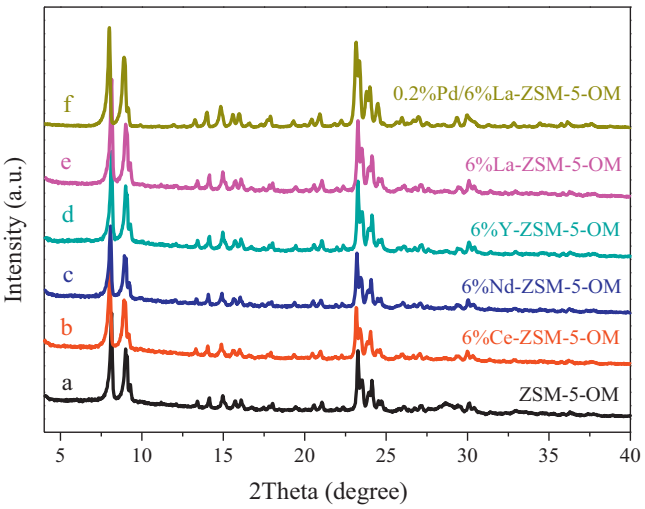

Fig. 1. XRD patterns of (a) ZSM-5-OM, (b) 6%Ce-ZSM-5-OM, (c) 6%Nd-ZSM-5-OM, (d) 6%Y-ZSM-5-OM, (e) 6%La-ZSM-5-OM and (f) 0.2%Pd/6%La-ZSM-5-OM.

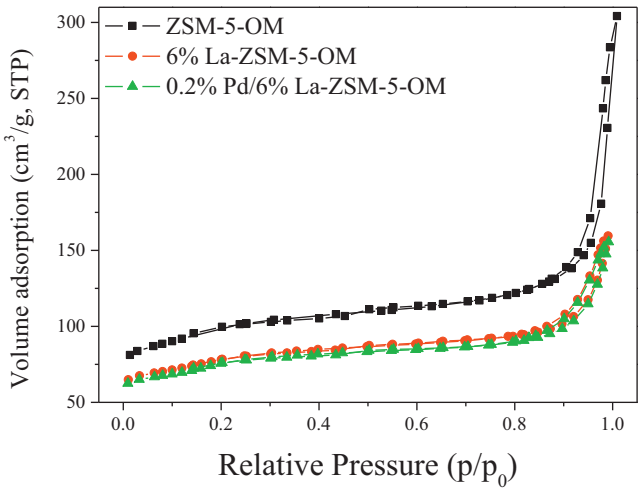

Fig. 2. N_2 isotherms of (a) ZSM-5-OM, (b) 6%La-ZSM-5-OM and (c) 0.2%Pd/6%La-ZSM-5-OM.

for 0.5 h under air condition, then the temperature was decreased to −30 °C. The reductive gas was a mixture of 5 vol% H_2 in Ar (40 mL/min), which was purified using deoxidizer and silica gel. The temperature of the sample was programmed to increase at a constant rate of 10 °C/min. The hydrogen uptakes during the reduction was measured by a thermal conductivity detector (TCD), and the effluent H_2O formed during H_2–TPR was absorbed with a 5 A molecular sieve.

2.4.1. Catalysts activity determination

Benzene was combusted in a microreactor at a space velocity of 20,000 h^{-1}. Reactive flow (125 mL/min) was composed of air and gaseous benzene (1000 ppm). The catalyst (40–60 mesh) was loaded in a quartz reactor and the bed volume was about 0.375 mL. Benzene conversion was analyzed by on-line gas chromatography (Shimadzu, GC–14 C) with a SE-30 capillary column.

3. Results and discussion

Fig. 1 shows the X-ray diffraction patterns of ZSM-5-OM and *x*%Pd/*x*%M-ZSM-5-OMs. Clearly, ZSM-5-OM showed several well-resolved peaks associated with the characteristic of MFI zeolite structure ranged from 4 to 40°, which confirmed the highly degree of crystallinity of ZSM-5-OM even after introduction of abundant *b*-aligned mesopores channels [28]. After impregnation of various metal oxides active species including Y, Ce, La, Pr, Nd and noble metal of Pd in ZSM-5-OM, giving the samples of *x*%Pd/*x*%M-ZSM-5-OMs, which still showed very good MFI zeolite structure, indicating good stability of ZSM-5-OM for supporting various metal oxides active species. It should be noted here that the peaks associated with the active sites of various metal oxides could not be observed in *x*%Pd/*x*%M-ZSM-5-OMs, which should be attributed to very low diffraction intensities of active species in comparison with that of ZSM-5-OM support. The low diffraction intensities of active species in *x*%Pd/*x*%M-ZSM-5-OMs resulted from their low contents and good dispersion of active species [29].

Fig. 2 shows N_2 sorption isotherms of ZSM-5-OM, 6%La-ZSM-5-OM and 0.2%Pd/6%La-ZSM-5-OM. Clearly, all of the samples exhibited type-IV N_2 sorption isotherms with hysteresis loops at relative pressures (P/P_0) of 0.85–0.95, indicating the presence of mesopores in these samples [28]. Correspondingly, the pore volumes of ZSM-5-OM, 6%La-ZSM-5-OM and 0.2%Pd/6%La-ZSM-5-OM were 0.279, 0.202 and 0.197 cm^3/g, respectively, and the pore diameter of ZSM-5-OM, 6%La-ZSM-5-OM and 0.2%Pd/6%La-ZSM-5-OM were distributed at 17.9, 14.3 and 14.9 nm, respectively (As shown in Table 1). Compared with ZSM-5-OM, the decreased, BET surface areas, pore volumes and pore diameters in 6%La-ZSM-5-OM and 0.2%Pd/6%La-ZSM-5-OM should be attributed to the increase density of network and block mesopores of ZSM-5-OM by PdO and La_2O_3 active species, similar results have also been reported previously [29]. It should be noted here that abundant and controlled mesoporosity in ZSM-5-OM support was favorable for good dispersion of active species and fast diffusion of reactants, which largely enhance their catalytic performances in various reactions.

Fig. 3 shows the SEM and EDX images of 0.2%Pd/6%La-ZSM-5-OM. Clearly, 0.2%Pd/6%La-ZSM-5-OM exhibits single crystal morphology with hexagonal prism shape, giving the crystal sizes at around 3 × 5 μm (Fig. 3 A&B). The unique single crystal structure usually results in their good stability for loading with various active species. Interestingly, the high resolution SEM images showed that 0.2%Pd/6%La-ZSM-5-OM had rough surface morphology and abundant mesoporosity, which are arranged along *b*-axis, running through the whole ZSM-5-OM crystals (Fig. 3C and D), in agreement with results reported by us previously [28]. Correspondingly, the EDX images showed the signals of Si, Al, Pd, La and O, suggesting that the active species of Pd and La have

Table 1
Structural parameters of ZSM-5-OM, 6%La-ZSM-5-OM and 0.2%Pd/6%La-ZSM-5-OM.

Samples	S_{BET} (m^2/g)	Mesopore size (nm) [a]	V_p [b] (cm^3/g)	V_{mic} (cm^3/g)
ZSM-5	371	–	0.14	0.13
ZSM-5-OM	330	17.9	0.279	0.074
6%La-ZSM-5-OM	269	14.3	0.202	0.058
0.2%Pd/6%La-ZSM-5-OM	261	14.9	0.197	0.051

[a] Pore size distribution estimated from BJH model.
[b] Pore volumes of the samples were estimated through N_2 isotherms at relative pressure of $p/p_0 = 0.94$.

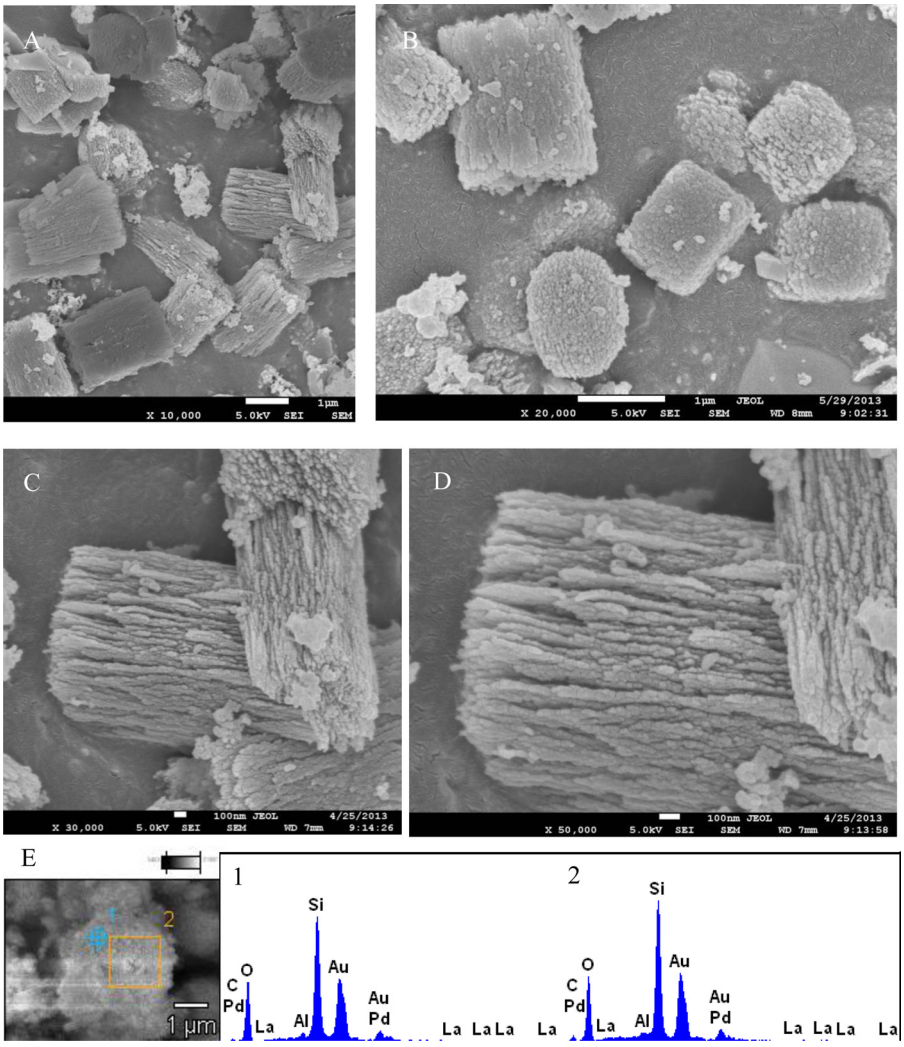

Fig. 3. SEM images of (A–D) and (E) EDX images of 0.2%Pd/6%La-ZSM-5-OM.

been successfully loaded into ZSM-5-OM support. In addition, EDX elemental maps further confirm the presence of Si, O, La, Al and Pd in 0.2%Pd/6%La-ZSM-5-OM, which were homogeneously dispersed in 0.2%Pd/6%La-ZSM-5-OM (Fig. S1).

Fig. 4 shows TEM images of 0.2%Pd/6%La-ZSM-5-OM, which exhibits single crystal characteristics with *b*-axis-aligned mesopores (Fig. 4A–C), in good agreement with SEM results. On the other hand, the active species of PdO and La_2O_3 nanocrystals with the particle sizes ranged from 10 to 50 nm were homogeneously dispersed into the mesopores of 0.2%Pd/6%La-ZSM-5-OM. The good dispersion of active species in 0.2%Pd/6%La-ZSM-5-OM is attributed to its structural character of abundant and *b*-axis-aligned mesopores, which results in their high exposition degree and good anti aggregation of active species during catalytic reactions. In order to reveal the nanostructure of active species in 0.2%Pd/6%La-ZSM-5-OM, the high resolution TEM images of 0.2%Pd/6%La-ZSM-5-OM have also been investigated, which showed good nanocomposition PdO and La_2O_3 active species, giving several nanocrystallites with well-defined lattice planes (Fig. 4D and E), suggesting a high degree of crystallinity of active species in 0.2%Pd/6%La-ZSM-5-OM.

Fig. 5 shows X-ray photoelectron spectroscopy measurements of 0.2%Pd/6%La-ZSM-5-OM, which was an efficient tool for characterization of surface active sites of solid catalysts. 0.2%Pd/6%La-ZSM-5-OM showed several peaks associated with Al, Si, O, Pd and La, indicating the successful loading of Pd and La active species in ZSM-5-OM support (Fig. 3A), which was also confirmed by EDX images (Fig. S1). To further understand the detailed characters of the active sites in 0.2%Pd/6%La-ZSM-5-OM, high-resolution XPS spectra of O, Pd and La have also been investigated (Fig. 3B–D). The Pd spectrum showed two peaks associated with $Pd3d_{3/2}$ and $Pd3d_{5/2}$ at around 336.9 and 342.1 eV, respectively, which were assigned to Pd^{2+} species, indicating presence of PdO in 0.2%Pd/6%La-ZSM-5-OM (Fig. 2B) [38–40]; On the other hand, the La spectrum showed several peaks ranged from 830 to 860 eV associated with $La3d_{3/2}$ and $La3d_{5/2}$, which were assigned to La^{3+} species, indicating presence of La_2O_3 in 0.2%Pd/6%La-ZSM-5-OM (Fig. 2D). Furthermore, the peak associated with O1s ranged from 530 to 535 eV indicates presence of active oxygen species (*e.g.* O^- and O_2^- species), which may be attributed to a large amount of oxygen vacancies existing in the structure of samples (Fig. 2C) [29,41,42]. The successfully loading of PdO and La_2O_3 active species in ZSM-5-OM plays key factor for its superior catalytic activity for benzene combustion.

Fig. 6 shows H_2-temperature program reduction (H_2–TPR) curves of various samples, which was an efficient way to characterize the oxidation abilities of various catalysts. Notably, 0.2%Pd/6%La-ZSM-5-OM showed several peaks at around 15.8 and 50.3 °C, and 351.7 and 640.3 °C, which should be attributed to the reduction of various active species in 0.2%Pd/6%La-ZSM-5-OM; The lower reduction temperatures at around 15.8 and 357.1 °C

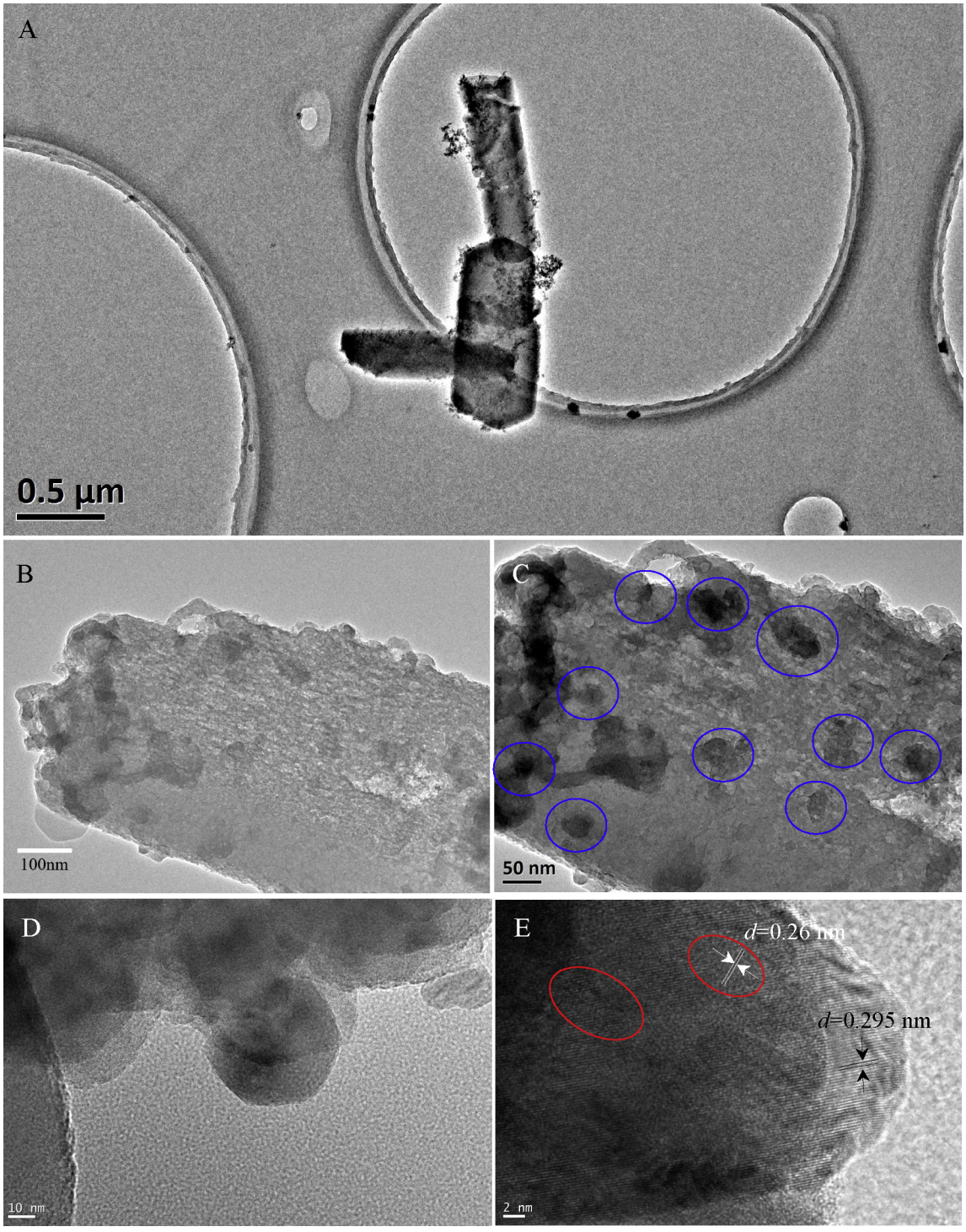

Fig. 4. (A–C) TEM and (D and E) high resolution TEM (HR-TEM) images of 0.2%Pd/6%La-ZSM-5-OM.

may be attributed to the reactions of H_2 with PdO nanocrystals and nanosized La species (*e.g.* La-carbonate or oxyhydride) or adsorbed active oxygen species; While the higher reduction temperatures at around 50.3 and 640.3 °C may be attributed to reaction of H_2 with bulky PdO and La species, which were located on the surface of ZSM-5-OM support. It should also be noted here that the presence of negative peaks at around 83.5, 84.6 and 88.7 °C in PdO containing samples including 0.2%Pd/6%La-ZSM-5-OM, 0.2%Pd/6%La-ZSM-5 and 0.2%Pd/ZSM-5-OM may be attributed to the decomposition of PdH_2, which formed during H_2–TPR tests and decomposed at around 80–90 °C. The decomposition of PdH_2 will release H_2 (meaning H_2 evolution), further resulting in negative peaks in these samples.

Interestingly, the reaction temperatures of La species (536.9 and 764.5 °C) with H_2 in 6%La-ZSM-5-OM were much higher than those of 0.2%Pd/6%La-ZSM-5-OM (357.1 and 640.3 °C), which should be attributed to the unique interactions between PdO and La species in 0.2%Pd/6%La-ZSM-5-OM [29]. Furthermore, the unique interactions between PdO and La species also result in the increased reduction temperatures of PdO (15.8 and 50.3 °C) in 0.2%Pd/6%La-ZSM-5-OM in comparison with that of 0.2%Pd/ZSM-5-OM (10.9 and 43.8 °C). On the contrary, the reaction temperatures of both

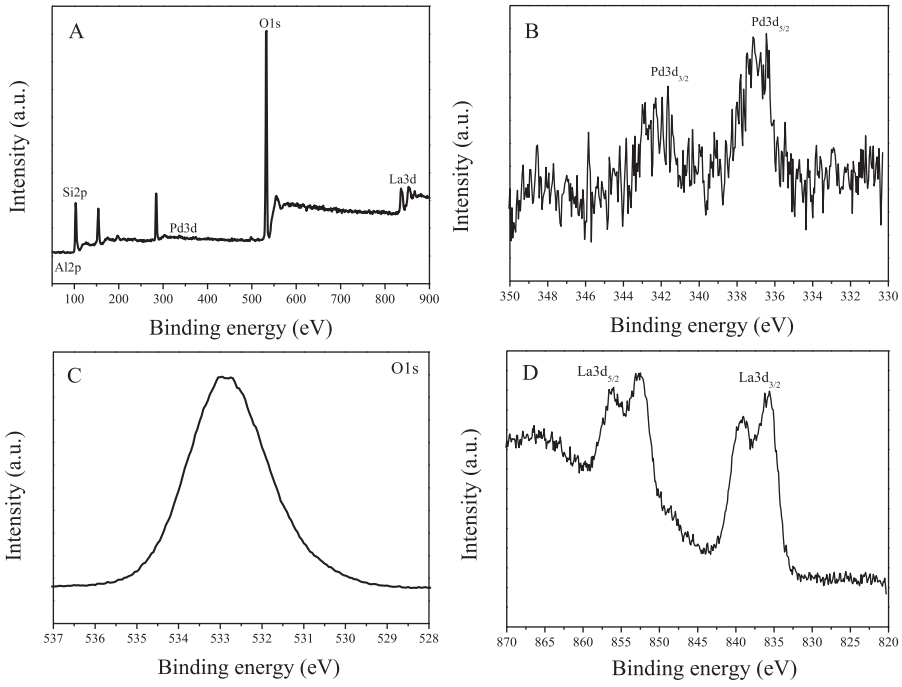

Fig. 5. XPS spectra of (A) survey, (B) Pd_{3d}, (C) O_{1s} and (D) La_{3d} of 0.2%Pd/6%La-ZSM-5-OM.

PdO and La species with H_2 in 0.2%Pd/6%La-ZSM-5 were obviously higher than those of 0.2%Pd/6%La-ZSM-5 (As shown in Fig. 6a and d). Consideration of the interactions between PdO and La active species existed in both 0.2%Pd/6%La-ZSM-5-OM and 0.2%Pd/6%La-ZSM-5, the higher reduction temperatures of PdO and La species in 0.2%Pd/6%La-ZSM-5 may be attributed to their large particle sizes and bad dispersion, which result from poor mesoporosity in ZSM-5 support. The low reduction temperatures of PdO and La species in 0.2%Pd/6%La-ZSM-5-OM was favorable for the enhancement of its catalytic activities for VOCs oxidation, similar results have not been reported for functional mesoporous zeolites previously.

Fig. 7 shows the dependences of catalytic activities on reaction temperatures for benzene combustion over various catalysts including Y, Ce, La, Pr and Nd metal oxides functionalized 0.2%Pd/ZSM-5-OM, which was a typical reaction in the area of VOCs oxidation. Notably, 0.2%Pd/6%La-ZSM-5-OM exhibited the best catalytic activities, which gave the lowest temperature for full oxidation of benzene as low as 270 °C (Fig. 7), much better than that of 0.2%Pd/6%La-ZSM-5 (Figure S2); To further reveal the relationship between catalytic activities and contents of various active species, we have also carefully tested catalytic activities of *x*%Pd/*x*%M-ZSM-5-OMs with different contents of Pd or La for benzene combustion under the same conditions (Figs. 8 and 9). Interestingly, *x*%Pd/*x*%La-ZSM-5-OMs with the compositions of 0.6%Pd and 6%La exhibited the best catalytic activities, which showed the lowest temperature for benzene combustion to be as low as 220 °C, much lower than various results reported previously [43]. Further increasing the contents of active species of Pd or La may lead to partial aggregation of active sites and blocking of mesopores of *x*%Pd/*x*%La-ZSM-5-OM, which result in their decreased catalytic activities (Fig. 8 & 9). The excellent catalytic activities of 0.6%Pd/6%La-ZSM-5-OM for benzene combustion

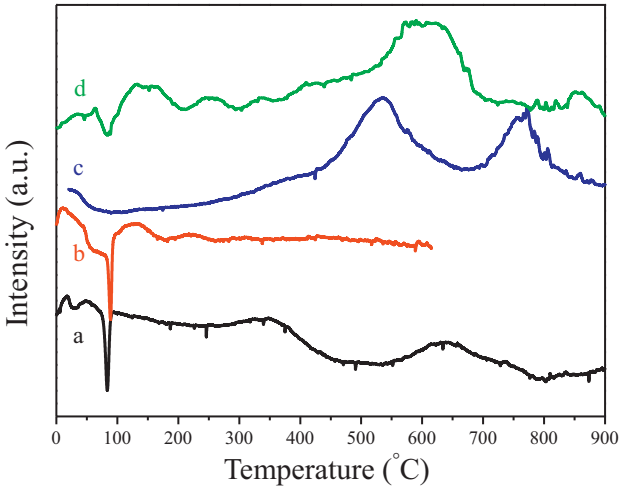

Fig. 6. H_2-temperature program reduction (H_2-TPR) curves of (a) 0.2%Pd/6%La-ZSM-5-OM, (b) 0.2%Pd/ZSM-5-OM, (c) 6%La-ZSM-5-OM and (d) 0.2%Pd/6%La-ZSM-5.

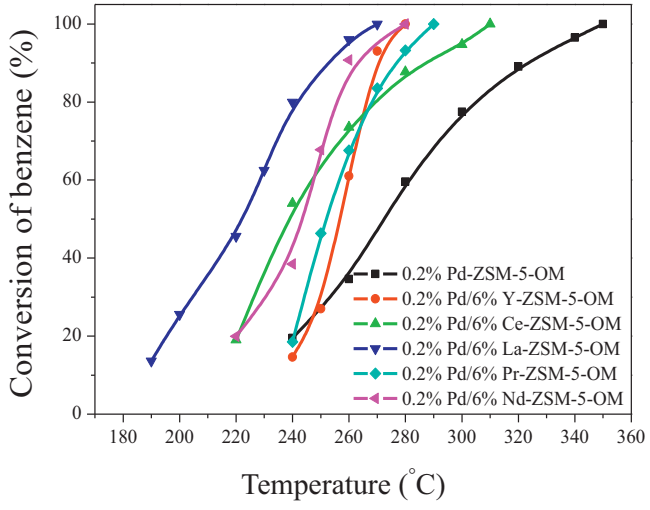

Fig. 7. Dependences of catalytic activities on reaction temperatures for benzene combustion over various samples of 0.2%Pd/ZSM-5-OM, 0.2%Pd/6%Y-ZSM-5-OM, 0.2%Pd/6%Ce-ZSM-5-OM, 0.2%Pd/6%La-ZSM-5-OM, 0.2%Pd/6%Pr-ZSM-5-OM and 0.2%Pd/6%Nd-ZSM-5-OM.

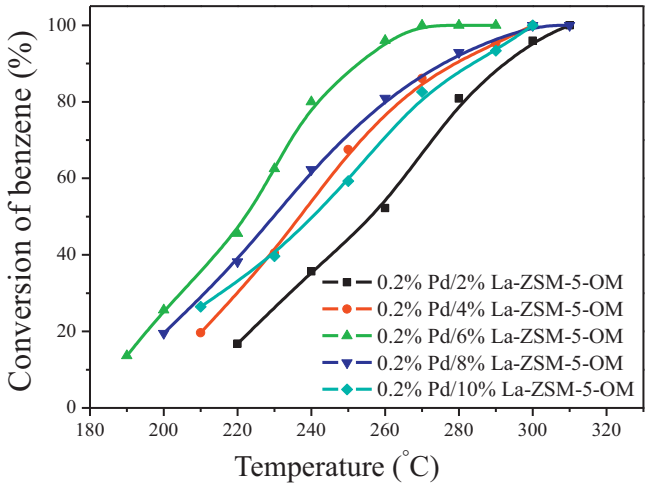

Fig. 8. Dependences of catalytic activities on reaction temperatures for benzene combustion over different contents of LaO_x loaded in 0.2%Pd/ZSM-5-OM.

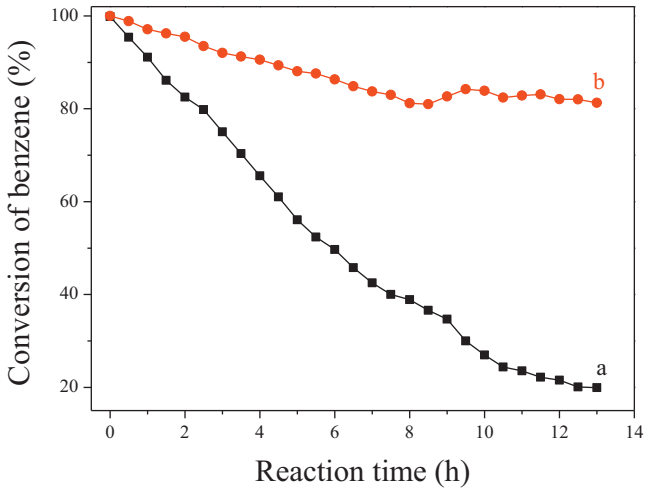

Fig. 10. Dependences of catalytic activities on reaction time for benzene combustion at 240 °C over (a) 0.6%Pd/6%La-ZSM-5 and (b) 0.6%Pd/6%La-ZSM-5-OM.

should be assigned to their novel characters including abundant and *b*-axis-aligned mesoporosity, good dispersion and small PdO and La_2O_3 nanocrystals, and unique interactions between PdO and La_2O_3 in 0.6%Pd/6%La-ZSM-5-OM.

Fig. 10 shows the dependences of catalytic activities for benzene combustion on reaction time over 0.6%Pd/6%La-ZSM-5 and 0.6%Pd/6%La-ZSM-5-OM at 240 °C. Clearly, both fresh 0.6%Pd/6%La-ZSM-5-OM and 0.6%Pd/6%La-ZSM-5 showed full oxidation of benzene. After increasing of the reaction time to 8 h, 0.6%Pd/6%La-ZSM-5-OM showed a decreased conversion of benzene at 81.5%; In contrast, the conversion of benzene catalyzed by 0.6%Pd/6%La-ZSM-5 was only 38.8%. With further increase of the reaction time up to 13 h, there was nearly no loss of activity for 0.6%Pd/6%La-ZSM-5-OM, which still gave the conversion of benzene up to 81.4%; While 0.6%Pd/6%La-ZSM-5 showed only 20.2% conversion of benzene. These data confirmed the long-lived catalytic property of 0.6%Pd/6%La-ZSM-5-OM in comparison with 0.6%Pd/6%La-ZSM-5 for benzene combustion. Compared with 0.6%Pd/6%La-ZSM-5, the longer catalytic life of 0.6%Pd/6%La-ZSM-5-OM for benzene combustion may be attributed its much improved anti-sintering ability of PdO and La_2O_3 nanocrystals in ZSM-5-OM support, which resulted from its novel *b*-axis-aligned mesopore channels, further resulting in the good dispersion and anti aggregation of PdO and La_2O_3 active species in 0.6%Pd/6%La-ZSM-5-OM.

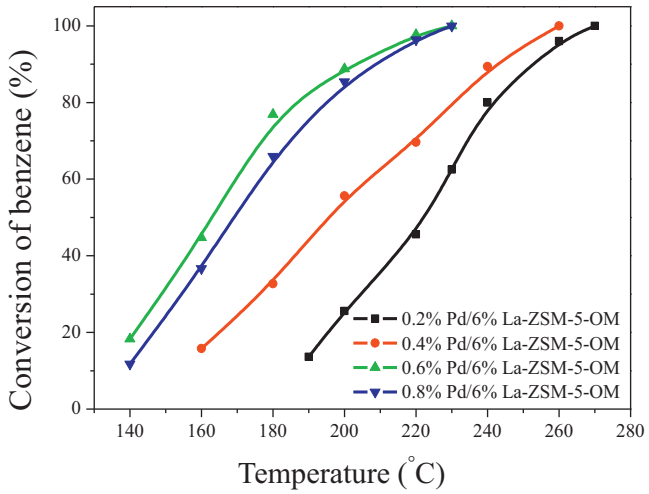

Fig. 9. Dependences of catalytic activities on reaction temperatures for benzene combustion over different contents of PdO loaded in 6%La-ZSM-5-OM.

Collaboration of the novel features of 0.6%Pd/6%La-ZSM-5-OM including abundant and controlled *b*-axis-aligned mesopore channels, large BET surface areas, excellent catalytic activity and long catalytic lives for benzene oxidation, 0.6%Pd/6%La-ZSM-5-OM will open a new way for applications of functional hierarchical zeolites with controllable mesopores for VOCs combustion under green and mild conditions.

4. Conclusions

A series of Pd/transition metal oxides nanocrystals functionalized ZSM-5 single crystals with *b*-axis-aligned mesoporous channels have been successfully prepared in this work, *x*%Pd/*x*%M-ZSM-5-OMs showed novel characters including abundant and controllable mesopores, good dispersion of active species and unique interactions between Pd and transition metal oxides, which result in their excellent catalytic activities and very long catalytic lives for benzene combustion under green and mild conditions (220 °C). The preparation of *x*%Pd/*x*%M-ZSM-5-OMs will develop efficient and stable solid catalysts with controlled nanoporosity and excellent catalytic performances for VOC's for removing under green and mild conditions, which will be potentially important for environmental protection in our daily lives.

Acknowledgments

This work was supported by the National Natural Science Foundation of China (21203122), the Foundation of Science and Technology of Shaoxing Bureau (2012B70018), Key Sci-Tech Innovation Team Project of Zhejiang Province (2010R50014-20), China and Postdoctoral Foundation of China (2012M520062).

Appendix A. Supplementary data

Supplementary data associated with this article can be found, in the online version, at http://dx.doi.org/10.1016/j.apcatb.2013.10.054.

References

[1] M.E. Davis, Nature 417 (2002) 813–821.
[2] M. Hartmann, Angew. Chem. Int. Ed. 43 (2004) 5880–5882.
[3] D.W. Breck, Zeolite Molecular Sieves, Structure, Chemistry and Use, John Wiley & Sons, New York, NY London, Sydney, Toronto, 1974.
[4] R.R. Xu, W.Q. Pang, J.H. Yu, Q.S. Huo, J.S. Chen, Chemistry of Zeolites and Related Porous Materials, Wiley, Singapore, 2007.

[5] H. van Bekkum, E.M. Flanigen, P.A. Jacobs, J.C. Jansen, Introduction to Zeolite Science and Practice, Elsevier, Amsterdam, 2001.
[6] D.W. Breck, Zeolite Molecular Sieves, Krieger, Malabar, 1984.
[7] A. Corma, Chem. Rev. 97 (1997) 2373–2419.
[8] M. Choi, K. Na, J. Kim, Y. Sakamoto, O. Terasaki, R. Ryoo, Nature 461 (2009) 246–249.
[9] J.X. Jiang, J.L. Jorda, J.H. Yu, L.A. Baumes, E. Mugnaioli, M.J. Diaz-Cabanas, U. Kolb, A. Corma, Science 333 (2011) 1131–1134.
[10] X.D. Zou, T. Conradsson, M. Klingstedt, M.S. Dadachov, M. O'Keeffe, Nature 437 (2005) 716–719.
[11] B.J. Schoeman, J. Sterte, J.E. Otterstedt, Zeolites 14 (1994) 110–116.
[12] L. Tosheva, V.P. Valtchev, Chem. Mater. 17 (2005) 2494–2513.
[13] M. Choi, H.S. Cho, R. Srivastava, C. Venkatesan, D.-H. Choi, R. Ryoo, Nat. Mater. 5 (2006) 718–723.
[14] Y. Tao, H. Kanoh, L. Abrams, K. Kaneko, Chem. Rev. 106 (2006) 896–910.
[15] X.J. Meng, F. Nawaz, F.-S. Xiao, Nano Today 4 (2009) 292–301.
[16] W. Fan, M.A. Snyder, S. Kumar, P.S. Lee, W.C. Yoo, A.V. McComick, P.L. Penn, A. Stein, M. Tsapatsis, Nat. Mater. 7 (2008) 984–991.
[17] H. Wang, T.J. Pinnavaia, Angew. Chem. Int. Ed. 45 (2006) 7603–7606.
[18] F.-S. Xiao, L.F. Wang, C.Y. Yin, K. Lin, Y. Di, J. Li, R. Xu, D. Su, R. Schlögl, T. Yokoi, T. Tatsumi, Angew. Chem. Int. Ed. 45 (2006) 3090–3093.
[19] C.J.H. Jacobsen, C. Madsen, J. Houzvicka, I. Schmidt, A. Carlsson, J. Am. Chem. Soc. 122 (2000) 7116–7117.
[20] H.Y. Chen, J. Wydra, X.Y. Zhang, P.-S. Lee, Z.P. Wang, W. Fan, M. Tsapatsis, J. Am. Chem. Soc. 133 (2011) 12390–12393.
[21] Z.X. Yang, Y.D. Xia, R. Mokaya, Adv. Mater. 16 (2004) 727–732.
[22] Y.S. Tao, H. Kanoh, K. Kaneko, J. Am. Chem. Soc. 125 (2003) 6044–6045.
[23] K. Na, M. Choi, W. Park, Y. Sakamoto, O. Tarasaki, R. Ryoo, J. Am. Chem. Soc. 132 (2010) 4169–4177.
[24] K. Na, C. Jo, J. Kim, K. Cho, J. Jung, Y. Seo, R.J. Messinger, B.F. Chmelka, R. Ryoo, Science 333 (2011) 328–332.
[25] Y. Seo, K. Cho, Y. Jung, R. Ryoo, ACS Catal. 3 (2013) 713–720.
[26] W. Kim, J.-C. Kim, J. Kim, Y. Seo, R. Ryoo, ACS Catal. 3 (2013) 192–195.
[27] J. Kim, W. Kim, Y. Seo, J.-C. Kim, R. Ryoo, J. Catal. 301 (2013) 187–197.
[28] F.J. Liu, T. Willhammar, L. Wang, L.F. Zhu, Q. Sun, X.J. Meng, W. Carrillo-Cabrera, X.D. Zou, F.-S. Xiao, J. Am. Chem. Soc. 134 (2012) 4557–4560.
[29] F.J. Liu, S.F. Zuo, X.D. Xia, Y.C. Zou, L. Wang, C.G. Li, C.Z. Qi, J. Mater. Chem. A 1 (2013) 4089–4096.
[30] M.-F. Luo, J.-M. Ma, J.-Q. Lu, Y.-P. Song, Y.-J. Wang, J. Catal. 246 (2007) 52–59.
[31] S.F. Zuo, Q.Q. Huang, J. Li, R.X. Zhou, Appl. Catal., B 91 (2009) 204–209.
[32] R. Atkinson, Atmos. Environ. 34 (2000) 2063–2101.
[33] P.O. Larsson, A. Andersson, L.R. Wallenberg, B. Svensson, J. Catal. 163 (1996) 279–293.
[34] Q.Q. Huang, S.F. Zuo, R.X. Zhou, Appl. Catal., B 95 (2010) 327–334.
[35] M. Labaki, S. Siffert, J.-F. Lamonier, E.A. Zhilinskaya, A. Aboukaïs, Appl. Catal., B 43 (2003) 261–271.
[36] P. Papaefthimiou, T. Ionnides, X.E. Verykios, Appl. Catal., B 13 (1997) 175–184.
[37] M. Guinet, P. Dégé, P. Magnoux, Appl. Catal., B 20 (1999) 1–13.
[38] M.B. Katz, G.W. Graham, Y.W. Duan, H. Liu, C. Adamo, D.G. Schlom, X.Q. Pan, J. Am. Chem. Soc. 133 (2011) 18090–18093.
[39] G. Ketteler, D.F. Ogletree, H. Bluhm, H.J. Liu, E.L.D. Hebenstreit, M. Salmeron, J. Am. Chem. Soc. 127 (2005) 18269–18273.
[40] K. Paredis, L.K. Ono, F. Behafarid, Z.F. Zhang, J.C. Yang, A.I. Frenkel, B.R. Cuenya, J. Am. Chem. Soc. 133 (2011) 13455–13464.
[41] W.P. Ding, Y. Chen, X.C. Fu, Catal. Lett. 23 (1994) 69–78.
[42] J. Liu, Z. Zhao, C.-M. Xu, A.-J. Duan, G.-Y. Jiang, J. Phys. Chem. C 112 (2008) 5930–5941.
[43] D. Delimaris, T. Ioannides, Appl. Catal., B 84 (2008) 303–312.